13

Determination of Internal Stresses in Lightweight Metal Matrix Composites

Guillermo Requena[1], Gerardo Garcés[2],
Ricardo Fernández[2] and Michael Schöbel[1]
[1]*Institute of Materials Science and Technology, Vienna University of Technology*
[2]*Department of Physical Metallurgy, National Center for Metallurgical Research-C.S.I.C.*
[1]*Austria*
[2]*Spain*

1. Introduction

Internal stresses are those stresses found in a body when this is stationary and in equilibrium with its surroundings (Withers & Badeshia, 2001). These stresses can arise at different length scales within a microstructure ranging from the size of the analysed body down to the atomic scale. Multiphase materials are prone to develop internal stresses due to the different mechanical and physical properties usually found between the phases that form these materials. This is essential for composites because the distribution and magnitude of the internal stresses may determine their mechanical/physical behaviour. Neutron diffraction has become an essential tool to determine internal stresses non-destructively in metal-based composite materials. The present chapter gives a thorough description of the state of the art of the technique and its use to determine internal stresses developed in lightweight metal matrix composites under mechanical, thermal and thermo-mechanical loading.

2. Metal matrix composites

The term composite material refers, in a first approach, to all kinds of materials systems composed of more than one solid phase. However, if we follow this definition, any alloy with a miscibility gap would have to be considered as a composite material since it is composed of two phases. To avoid this confusion, a more general and currently accepted definition of composite is the one provided in (mmc-assess.tuwien.ac.at):

A composite (or composite material) is defined as a material that consists of at least two constituents (distinct phases or combinations of phases) which are bonded together along the interface in the composite, each of which originates from a separate ingredient material which pre-exists the composite.

Following this definition, the composite is produced via a physical combination of at least two pre-existing ingredient materials. The so called in-situ composite materials are those where the pre-existing ingredients change their chemical composition or their shape during mixing. Those produced by reactions between elements or between compounds within the

material system (Tjong 2000) fall outside this definition. Although their properties can be described using composite theory (e.g. grey cast iron) they will not be considered as composite materials in the present work. As already stated, a composite presents at least two constituents, one of them may act as the matrix and the other one/s as the reinforcement/s. To complete our previous definition we define the components of the composite as follows:

The matrix of a composite refers to the phase which presents a continuous structure and usually, but not exclusively, is the phase with highest volume fraction. The other phases of the composite are called the reinforcement.

Composites can now be classified by means of the type of matrix they have. The matrices of technological interest are polymeric, metallic and ceramic matrices. Thus, we have three different types of composites:

- MMC: *Metal Matrix Composites*
- CMC: *Ceramic Matrix Composites*
- PMC: *Polymer Matrix Composites*

Now, we are able to give a consistent definition of metal matrix composites:

A Metal Matrix Composite (MMC) is a composite material in which one constituent, the matrix, is a metal or alloy forming at least one percolating network. The other pre-existing constituent or their derivatives are embedded in this metal matrix and play the role of reinforcement phases. In addition, it is convenient to limit the volume fractions of the constituents to be considered as MMC (mmc-assess.tuwien.ac.at): matrix volume fraction > 5% and reinforcement volume fraction > 5%.

2.1 Types of MMC

MMC are classified into two subgroups according to the architecture of the reinforcement:

1. Continuously reinforced MMC:
   - Monofilament reinforced metals (MFRM) (Fig. 1 a): monofilaments of approximately 0.1 mm in diameter (e.g. SiC) are embedded uni- or bidirectionally within a metallic matrix by diffusion bonding (Leyens et al., 2003; Brendel et al., 2007; Peters et al., 2010).
   - Continuous fibre reinforced metals (CFRM) (Fig. 1 b): uniaxial or multiaxial multifilament tows of at least some hundreds of fibres of about 0.01 mm in diameter (e.g. C, Al_2O_3) are embedded within a metallic matrix, usually, by infiltration methods.
   - Interpenetrating composite metals (ICM) (Fig. 1 c): percolating ceramic structures can also be used as continuous reinforcement resulting in an MMC in which both the matrix and the reinforcement are continuous phases forming an interconnected 3D structure throughout the volume.
2. Discontinuously reinforced MMC:
   - Particle reinforced metals (PRM) (Fig. 1 d): irregular or spherical particulates or platelets (e.g. SiC, Al_2O_3, B_4C) are embedded within the metallic matrix. Stir casting, infiltration and powder metallurgy (PM) are the usual processing routes used to produce PRM. Dispersion strengthened metals produced by powder metallurgy incorporating particles <1μm in size are frequently called nano-

composites, but contain usually <5 vol% of particles placing them outside of the definition of MMC.

- Short fibre reinforced metals (SFRM) (Fig. 1 e): short fibres (usually Al_2O_3) of high aspect ratio (length-to-diameter ratio) or whiskers (e.g. SiC) are embedded within the metallic matrix. SFRM are usually produced by infiltration of randomly distributed short fibre preforms. Strengthening is only provided by over-critical volume fractions of short fibers, usually >5 vol%. Whiskers have been forbidden in Europe due to their asbestos-like toxicity (Birchal et al., 1988).). The harmfulness of carbon nano tubes (CNT) is still in discussion, but it is hardly possible to achieve a uniform distribution of > 5 vol% of CNT within a metal matrix. The verification of an increase in stiffness by CNT needs further research, whereas the strength increase is mainly due to dispersion strengthening.

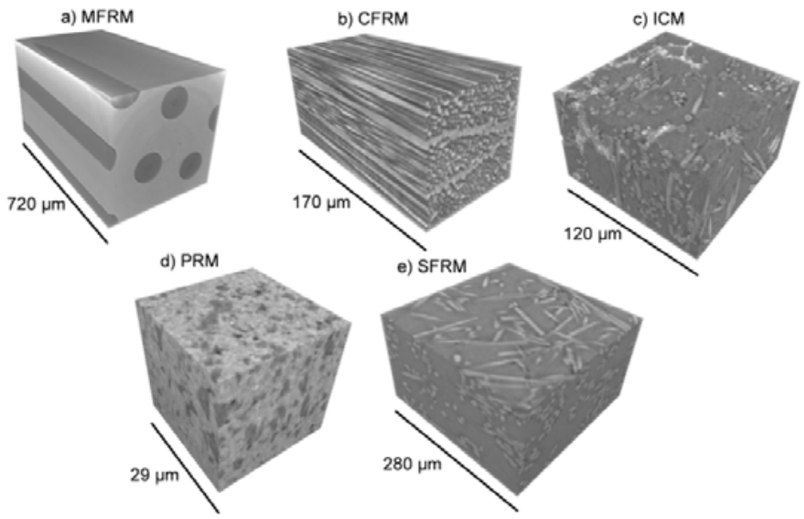

Fig. 1. Microstructures of different types of MMC revealed by synchrotron microtomography: a) SiC monofilament reinforced Cu (MFRM), b) Al matrix reinforced with continuous C fibres (CFRM), c) ICM formed by an Al matrix reinforced with an interpenetrating network of Al_2O_3 short fibres (light grey), eutectic Si (dark grey) and Ni- and Fe-rich aluminides (white), d) SiC particle reinforced 2124 Al-alloy (PRM) and e) Al_2O_3 short fibre reinforced Al matrix.

The possibility to combine light alloy matrices, i.e. Al-, Mg-, and Ti-alloys, with ceramic reinforcement has been a matter of technical interest during the last decades due to the increase in mechanical properties that lightweight MMC offer (Degischer, 1997), particularly regarding specific stiffness. This can be understood from the Ashby map (Ashby, 2005) in Fig. 2, where the Young's modulus of engineering metals and ceramics is shown as a function of their density. Guide lines for minimum mass design are introduced for the cases of bars under tensile / compressive loading, bending bars and for membranes. The E/ρ factor (specific modulus) for light alloys and steels is essentially the same (red dashed line). The only chance to increase the specific moduli of metals is by moving it towards the upper left corner (indicated by the arrow). The engineering ceramics are located in a region with a higher E/ρ but these materials are usually too brittle to be used for structural parts. Lightweight MMC appear as an innovative solution for this problem since they tailor the

properties of ceramic and metallic materials and can increase the specific stiffness of their matrices, as it is shown in Fig. 2 for the case of Al-based composites.

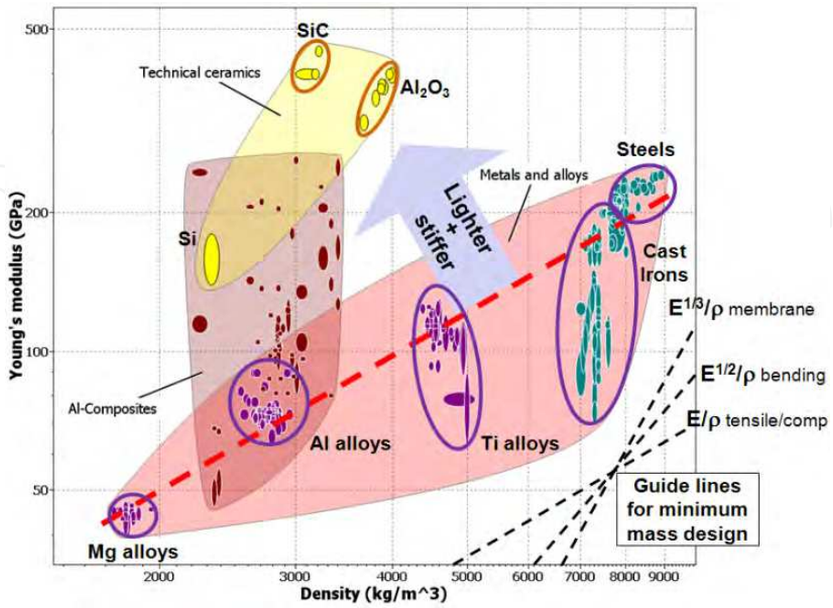

Fig. 2. Young's modulus vs density for engineering metals and some ceramics. The technical lightweight alloys are indicated together with the steels and cast irons. Guide lines for minimum mass design are included (CES Edupack, 2010)

3. Origins of internal stresses in materials

Internal stresses are those arisen in materials from shape misfits between different parts, regions or phases of materials and/or components. If no external load is acting on the considered body they are called residual stresses. Shape misfits are caused by different thermo-mechanical treatments. It is well established that almost every processing step during materials manufacture introduces residual stresses. For instance, machining, usually exemplified by a cold hole cutting in a sheet, strongly modifies the residual stress state of materials. Other cold deformation steps that introduce residual/internal stresses by mechanical working apart from cutting are bending, peening, cold laminating and cold forging. The resultant internal/residual stresses will depend on sample geometry, microstructure and process parameters such as magnitude and type of external applied stress, time, etc.

Other sources of residual stresses are temperature changes and temperature gradients. Thus, residual stresses may be introduced when materials or components are subjected to thermal treatments. These are very common in industrial processes, achieving its maximum significance for heat treatable alloys such as aluminum alloys of the 2xxx, 5xxx or 6xxx series. Thermal stresses can be divided in two main groups. The first one includes those treatments that produce strong residual stress profiles, e.g. quenching. They are usually introduced by sudden temperature variations on the sample that can result in the occurrence of plastic gradients within the body. The second group includes those heat treatments that relieve residual stresses, as for example annealing treatments.

Both thermal and mechanical effects usually appear simultaneously. The reason is that most of the manufacturing steps applied to metallic materials and components are composed of a combination of thermal and mechanical steps. Typical examples are hot forming and shape casting with mechanical constraints exerted by the tools. In these situations, it is not possible to separate the contributions of each individual process parameter and the resulting internal/residual stress distribution is usually very complex.

Furthermore, during service, internal stresses include residual stresses produced by thermal exposures of components, e.g. thermal cycling of multi-phase or multi-material systems.

3.1 Types and origin of internal stresses relevant to MMC

Internal stresses are normally divided in three categories depending on their length scale:

Type I – Macrostresses: these stresses are those acting over a length scale of the size of the considered body and are usually developed during processing and/or thermo-mechanical processing of the material. Among the thermal treatments, quenching processes are a paradigmatic example for the generation of this kind of stresses. In relation to mechanical processing, macrostresses appear in those steps that introduce plastic strain gradients such as shot-peening or bending. In this size range, anisotropy in the residual stress profile may be introduced depending on the geometry of the body. Fig. 3 illustrates the different types of internal stresses that can arise during extrusion of PRM. The cooling temperature profile generated after extrusion results in the development of a macrostress profile that goes from tensile stresses in the centre of the bar to compressive in the surface (Noyan and Cohen, 1987, Hutchings et al., 2005). It is important to point out that macrostresses are homogenous at least along one direction and that they must be balanced throughout the body, i.e.

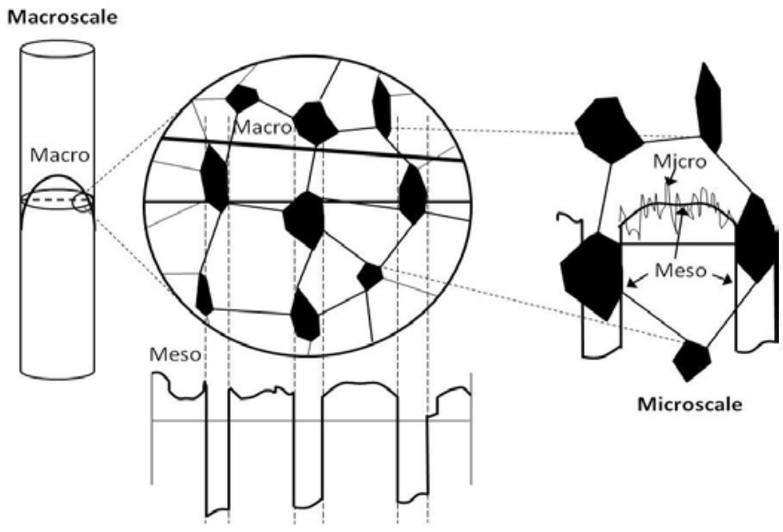

Fig. 3. Schematic view of the residual stresses that can arise in the different structural scales of a PRM. Ceramic particles are indicated as black regions.

$$\int_V \sigma_{ij} dV = 0 \tag{1}$$

where σ_{ij} represents the stress in direction ij and V is the volume of the body.

Macrostresses can be relieved by relaxation heat treatments or by plastic deformation.

Type II – Microstresses (also known as mesostresses): this kind of residual or internal stresses is originated from inhomogeneities in a material and thus is related to a length scale of the heterogeneity, e.g. the grain size, reinforcement size, interspacing between different phases, etc. They can arise due to several reasons, e.g. inhomogeneous distribution of plastic deformation on a micro scale, thermal/elastic mismatch between phases, crystallographic texture, etc. In the case of MMC, the different mechanical and physical properties of the component phases are sources of type II microstresses. Thus, the different thermal expansion coefficients between the metallic matrix and the ceramic reinforcement result in the generation of type II thermal microstresses during temperature variations. Furthermore, the load partitioning between matrix and reinforcement, typical of MMC, is in fact a type II microstresss. The following equation indicates the condition for the balance of type II microstresses in the absence of external loads,

$$\sum_{i=1}^{n} f_i \, \sigma_{jki} = 0 \tag{2}$$

where f is the volume fraction of the phase i and $<\sigma_{jk}>$ represents the mean microstress in the direction jk for the phase i. If an external load is applied the sum must be equal to this and equation (2) must be modified accordingly. Type II microstresses can be reduced by annealing or by plastic deformation. However, they can be more or less re-established after cooling or loading. For instance, thermal cycling of MMC is accompanied by reversible cyclic changes of mesostresses.

Type III – microstresses: these stresses are found in the smallest length scale, e.g. stress fields around dislocations or within dislocation entangles, intergranular stresses or stress field around solutes, vacancies or coherent precipitates. For the case of MMC, high dislocation density regions, called work hardened zones, can generate in the vicinity of the reinforcement during plastic deformation and temperature changes.

4. Neutron diffraction for non-destructive stress analysis

4.1 Why neutrons

Neutrons are nucleons without electric charge and with magnetic moment (s = ½). They interact strongly with the nuclei of atoms and with the magnetic moment of uncoupled electrons (Brückel et al. 2005; Pynn, 2011). Their deep penetration in solids (no Coulomb interaction) and their scattering potential give neutrons superior properties for diffraction (Fitzpatrick & Lodini, 2003) compared to electrons and photons. For thermal neutrons (~ 25 meV) the scattering centers ($Ø_{nucleus}$ ~ 10^{-15} m) can be assumed as infinitely small point potentials compared to the lattice distances (d ~ 10^{-10} m) and wavelengths used (Behrens, 2011). Geometrical effects of the scattering center can be neglected. The scattering cross sections, which are independent of the atomic number Z, can be useful and restrictive as well, especially for some engineering materials with a negative scattering length (high incoherent background) such as Li, Ti and Mn. Besides their sophisticated radiation properties, the main problem with neutrons is their availability in terms of sources (Pynn,

2011). In fission reactors thermal neutrons are extracted from a "cloud" source with a diameter adequate to their slowing-down length (L_s ~ 30 cm) in the moderator (D_2O). These continuous sources use only a small fraction from the initial intensity of ~ 10^{15} n cm^{-2} s^{-1}. Primary monochromators reduce the flux on the sample to ~ 10^7 n cm^{-2} s^{-1}. Spallation sources (Carpenter, 2008) generate polychromatic neutron beams by proton acceleration and collision with a neutron emissive target reaching intensities of ~ 10^{17} n cm^{-2} s^{-1}. These pulsed sources, which are the most sophisticated neutron sources now available, are still not comparable to novel undulator or wiggler insertion devices at synchrotrons reaching photon fluxes of ~ 10^{30} ph cm^{-2} s^{-1}.

Neutron diffraction is particularly well suited to tackle the problem of three-dimensional strain measurement in unreinforced and reinforced materials for several reasons: due to their large penetration depth neutrons allow lattice strain measurements in the bulk of the specimen under investigation, thus avoiding unwanted surface effects; the orientation of the scattering vector with respect to the specimen axes can be changed arbitrarily by simple specimen manipulation, which is a prerequisite for three-dimensional stress analysis; the gauge volume can be adjusted to specific needs in the range from a few cubic millimetres to about a cubic centimetre without compromising the strain resolution. This is an important fact in materials with coarse grain size, since other non-destructive techniques (in particular synchrotron radiation diffraction) suffer from graininess.

4.2 Diffraction techniques

4.2.1 Angle dispersive neutron diffraction

Continuous neutron sources (fission reactors) emit thermal neutrons for diffraction with kinetic energies of ~ 25 meV (Brückel et al. 2005). Their wavelengths of λ ~ 1 – 2 Å is further restricted to a monochromatic neutron beam with a well defined λ. Si and Ge crystal arrays or bended single crystals are used as focusing monochromators which increase the intensity of the overall diffuse neutron radiation (thermal neutrons) to a high flux neutron beam directed towards the sample. Setups with fixed as well as with variable monochromator angle/wavelength can be used. An angle dispersive neutron diffraction experiment is shown schematically in Fig. 4. The neutron beam is diffracted by the polycrystalline sample producing Debye-Scherrer cones. A position sensitive detector system (PSD), usually a 2D ^{3}He detector array, acquires sections of these cones at preselected angles and distances (Brückel et al. 2005). The gauge volume in the sample is defined by primary and secondary slits. An angle dispersive diffraction measurement on an AlSi7/SiC/70p PRM (Schöbel et al., 2011) is shown in Fig. 5. The wavelength was set to 1.67 Å and the image in the detector shows the sections of the Debye-Scherrer cones of the Al(311) and SiC_{cubic}(311) crystallographic planes. The peak intensities are then vertically integrated over the PSD image and the d-spacing of the corresponding crystallographic plane can be calculated with the well-known Bragg's law,

$$d_{hkl} = \frac{n \cdot \lambda}{2 \cdot \sin\theta} \tag{3}$$

where n is a natural integer, and θ the diffraction angle (Fig. 5).

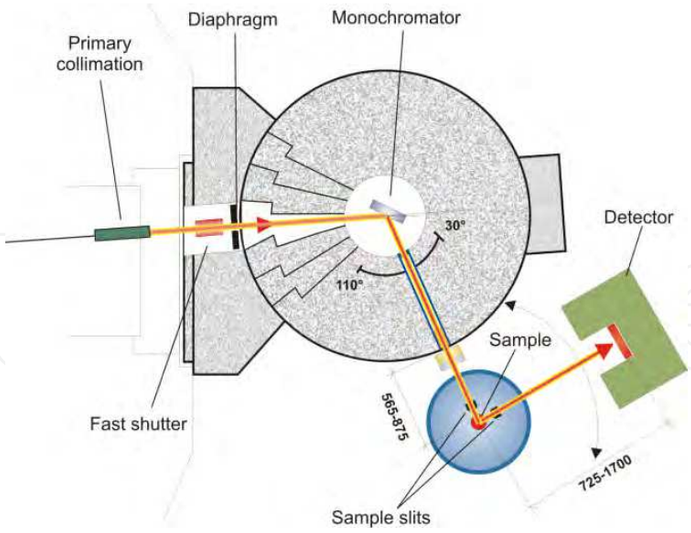

Fig. 4. Example of an angle dispersive neutron diffraction experiment using the Stress Spec instrument at the FRM II neutron source, Garching, Germany (www.frm2.tum.de).

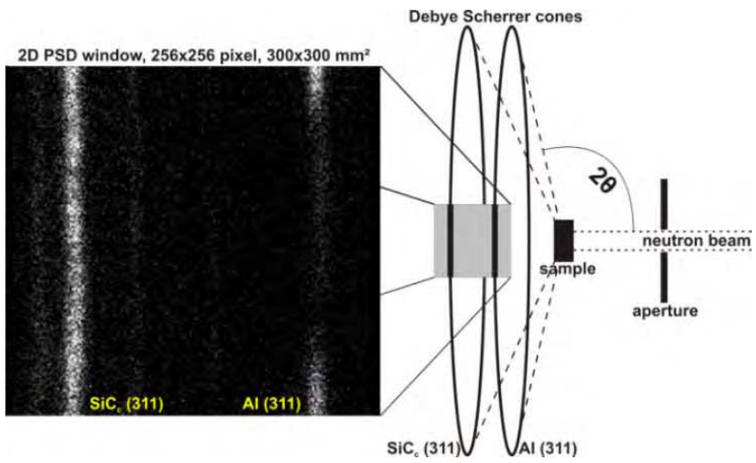

Fig. 5. Angle dispersive diffraction geometry and section of the Debye-Scherrer cones obtained by a monochromatic neutron beam scattered from an AlSi7/SiC/70p.

4.2.2 Time Of Flight neutron diffraction (TOF)

On pulsed neutron sources (spallation sources) a white neutron beam which covers a wide energy range (Santisteban, 2008) is used for diffraction. A polycrystalline sample diffracts all neutron wavelengths on all {h k l} lattice planes in space. Detector banks at two fixed positions from the sample (± 90°) cover two main strain axes of the sample in q_1 and q_2 direction (Fig. 6).

In a TOF strain scanner several neutron velocities are defined using a chopper in the primary beam. The wavelength of a neutron is given by the de Broglie relation $h \cdot \lambda = m \cdot v$, where h is the Planck's constant, m is the mass of the neutron and v is the velocity of the neutron. Furthermore, $v = t \cdot (L_1 + L_2)$, where t is the travelling time along well-known path lengths L_1 (distance source-sample) and L_2 (distance sample-detector). The lattice distances

can be determined using the Bragg's law depending on the travelling time at constant diffraction angle θ,

$$d_{hkl} = \frac{h}{2 \cdot \sin\theta \cdot m \cdot (L_1 + L_2)} \cdot t_{hkl} \tag{4}$$

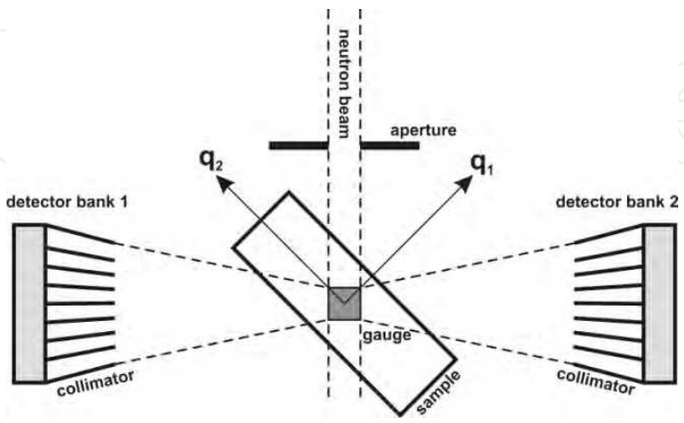

Fig. 6. TOF setup with two detector banks at fixed θ positions.

4.3 Neutron diffractometers for strain measurements

Table 1 shows an overview of the most important angle dispersive and time of flight neutron diffractometers available together with their main characteristics.

4.4 Some experimental issues

4.4.1 The d_0-problem

Neutron diffraction is a phase-sensitive strain measurement technique since it allows the determination of the average elastic strain acting in each microstructural phase independently. As a consequence, a reliable interpretation of the strain data depends greatly on the determination of a stress-free reference d_0 for each phase (see e.g. Fitzpatrick & Lodini, 2003). In principle, this can be achieved by investigating a stress-free reference sample (e.g. powders) using the same diffraction set-up. However, this can be affected by differences in composition between the reference and the studied materials due to different precipitation kinetics (this is typical for MMC (Dutta et al., 1991)), segregation during casting, etc. A description of several strategies to obtain d_0 is given for several cases in (Fitzpatrick & Lodini, 2003) but it must be kept in mind that this is a matter that presents serious difficulties for experimentalists. Some researchers have also reported methodologies that are independent of the measurement of a stress-free reference sample (Garcés et al., 2006; Young et al., 2007).

4.4.2 Systematic errors during strain measurement experiments

Some geometrical effects can influence the diffraction signal in angle dispersive diffraction. The intensity and position of the diffraction peak will depend not only on the internal stress state but also on absorption effects and the number and position of contributing crystals within the gauge volume that fulfil the Bragg condition.

Table 1.

Beamline / Facility	Flux on the sample	Sample size	Stage Type	In situ tests rigs	Experimental environment	Detector
Angle dispersive neutron diffraction						
STRESS-SPEC / FRM II (FR) (Hofmann et al., 2006; FRM II. STRESS-SPEC , 2011)	≤9.2×10^7 n s^{-1} cm^{-2} (graphite monocromator) ≤2×10^7 n s^{-1} cm^{-2} (Gemono-cromator)	max 300 kg	- Rotation table. - X Y Z translation table: x,y = ± 110 mm, z = 300 mm - 6 axis robot. - Eulerian cradles.	- 50 kN tension/compression rig (heatable to 1000 °C). -50 kN tension/comprssion + 100 Nm torsion rig.	- Variable take-off angle allows λ from 1.2Å– .4 Å - Mirror furnaces up to 1100 °C; Vacuum furnaces up to 1900 °C; Cryostats down to 30 mK.	Mirrotron MK-300-1; Gas mixture 3 bar ^{3}He + 2 bar CF_4; 300×300 mm^2 (256×256 pixel)
BT-8 / NIST NCNR (USA) (NIST, 2011)	~ 1 × 10^6 n $s^{-1}cm^{-2}$	- 0.6 m (h) x 0.6 m (w) x 1.0 m (l) - 100 kg	- Rotation table - Table with X Y Z -translation	- 10 kNrig, with table rotation in and tilt in Ψ, - 100 kNrig with rotation, combinable with 10 kNrigfor biaxial load.	Variable take-off angle allows λ= 0.9 Å – 3.0 Å withpossible $2\theta_{sample}\approx$ [40°,120°]	3He PSDactive area 10 cm x 5 cm (h)corresponding to approximately 8° width in 2θ
HB-2B/HFIR Oak Ridge National Laboratory (USA) (Oak Ridge National Laboratory, 2011)	≤ 3 × 10^7 n s^{-1} cm^{-2}	max. 450 kg	- XY translation / rotation table - Sample 400mm x 200mm; ≤ 1000 kg. - Z_1= 400 mm / 50 kg at 5 cm from stage;Z_2= 200 mm / 500 kg lift capacity from below. - ϕ rotation axis; Huber χ-ϕ full circle orienter,	- 22 kN Tension/compression load frame. - Tension/compression/torque - 4-point bending	- Furnaces (T). - User apparatus such as High Voltage field, gear loading apparatus.	Seven ORDELA 1155N PSD detectors covering 5° in the horizontal plane and +/- 15° from horizontal plane

Beamline / Facility	Flux on the sample	Sample size	Stage Type	In situ tests rigs	Experimental environment	Detector
G5-2 DIANE / LLB (FR) (LLB, 2011) (instr. being rebuild)	now~6.1x10^6 n cm^{-2} s^{-1}; future ~ 7.1x10^6 n cm^{-2} s^{-1}	max 300 kg max 1 m^3	- X Y Z translation table: - Eurelian cradle	- ± 25kNuni-axial tensile rig		100 x 100 mm^2 EMBL ^{5}He PSD
SALSA / ILL (FR) (Pirling et al., 2006; ILL, 2011)	Double focusing bent Si (400) monochromator, 2.5×10^7 n s^{-1} cm^{-2} at 1.6 Å, 0.25% Δd/d	- max length 1.5m - max -weight 700 kg	- Hexapod (Stewart platform, max tilt ±25°, x,y = ± 300 mm, z = ± 170 mm) - 90 Degree Eulerian cradle	- 10 kN vertical/horiz.mo untingrig for small samples; 50 kN horizontally mounting rig for static / dynamic tests. - 3kNthermo-mechanical rig; resistive heating T ≤ 1100 °C.	- Variable take-off angle allows λ from 1.3Å–2.4 Å - Variable optics (slits and radial collimators) Camera assisted metrology system	- 80 x 80 mm^2 2-dimensional Position Sensitive microstrip Detector.
E3 / HZB (D) (Wimpory et al., 2008; HZB, 2011)	~ 5 x 10^6 n cm^{-2} s^{-1}	max 250 kg	- -rotation table equipped with X Y Z - translation table - Eulerian cradles	Tensile, compressive and torsionmulti-axial load frame.	- cryostats (1.4K to 550 K); - furnaces (400K to 2000K); - Gas atmospheres	PSD ^{3}He Detector 30 x 30 cm^2
SMARTS / LUJAN LANL (USA) (Los Alamos, 2011)	n.a.	1 mm^3 - 1 m^3. max 1500 kg	- Rotation table (370°) - Table with X Y Z –translation (theodolites to position sample within 0.01 mm)	- 250 kN and at extreme T ≤ 1500°C. - Uniaxial 2 GPaloading on samples φ≤1 cm; with lower stresses T ≤ 1500°C.	- Cryogenics 200K to room temperature. - Up to 1800°C in stand alone configuration.	n.a.

Table 1.

Table 1.

Beamline / Facility	Flux on the sample	Sample size	Stage Type	In situ tests rigs	Experimental environment	Detector
Time of flight neutron diffraction						
ENGIN-X / ISIS (UK) (ISIS, 2011)	3×10^6 n $cm^{-2}s^{-1}$	- Capable for complex shape, - max 1000 kg	- X Y Z rotation table	- Stress rigs (up to 100 kN) can be equipped with furnce or cryostats (-200 °C – 1000 °C).	- Three types of furnaces: air or inert gas furnace can be equipped with stressrig (≤1100 °C), furnacewith ceramic heating pad and vacuum resistance furnace (≤1800 °C). - Cryostat down to -200°C	- For diffr. (2-θ at 90°): λ - shifting fibre coded Zn detector. - For Bragg edge transmission (2θ of 180°): 2D area detector / 10×10 scintillation detectors, each 2×2 mm^2 with 0.5 mm pitch.
SIRIUS / KENS (JP) (KENS, 2011)	n.a.	n.a.	n.a.	- 10 kN tensile stress machine	- Cryostat (7 K – RT). - Furnaces: RT-1000°C (vacuum, gas); 300 °C.	- 90° bank with 500 and 144 1D PSD (3He ½"x 60 cm)
POLDI / SINQ (CH) (PSI, 2011;Stuhr, 2005a; Stuhr, 2005b)	~10×10^7 n $cm^{-2}s^{-1}$ Thermal spectrum (1.1Å - 5Å)	- ≤ 10 ton - φ<450mm height<2000mm - Gauge vol.: $(0.6mm)^3$- $3.8 \times 30 \times 3.8 mm^3$	- 6 axis sample manipulator: X Y Z + rotation (360°) + 2-axis quarter cradle; Translation range vertical: 570mm Translation range horiz.:150mm<X, Y<150mm	- Tension-Compression, 20 kN, RT, mounting: vertical and horizontal - Rig under construction: 100 kN, multi-axial, RT to 1100 °C, LCF	standard furnaces (up to 1800 K); standard cryostats	He wire chamber; 2θ-range:30° ΔQ/Q: better 2×10^{-3} (Angular resolution: 0.075°; Time resolution: 1 μs) Radial collimators: 0.6mm; 1.5mm; 3.8mm

If large gauge volumes are used (≥ sample size) an absorption effect on the diffracted intensity must be taken into account (Fig. 7 a). The absorption gradient over the gauge volume causes a shift of the diffraction centre from the centre of gravity towards the primary beam. The consequence is an asymmetric peak shape. This effect differs for materials with different absorption characteristics as it is the case for the different phases in a MMC. Thus, relative peak shifts which are not caused by microstresses between the phases but by different absorption of the constituents may be observed.

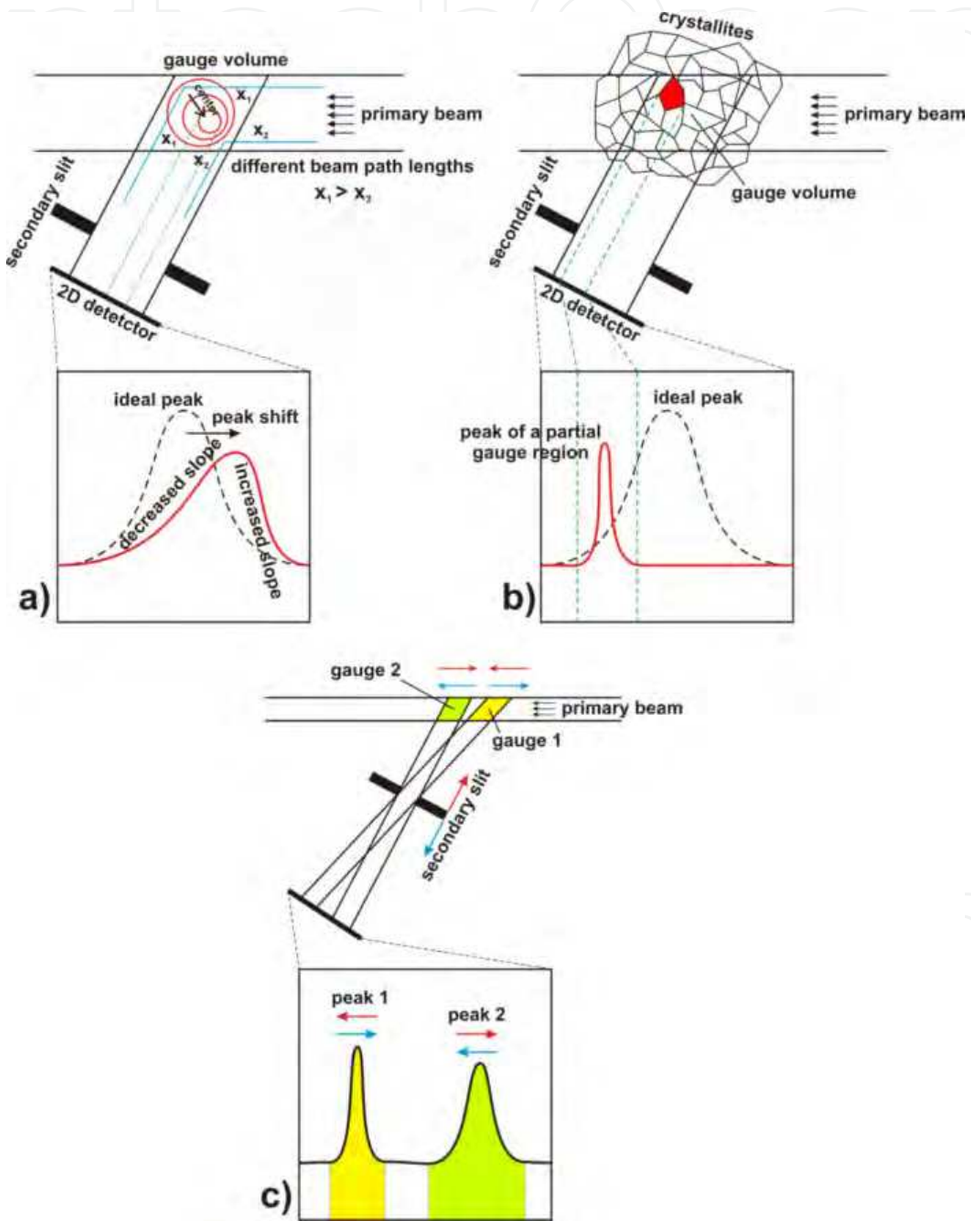

Fig. 7. Systematic errors that can occur using an angle dispersive diffraction setup (Schöbel, 2011a): a) displacement of the diffraction centre from the centre of the gauge volume due to absorption effects, b) coarse grains and c) pseudo micro strains generated by a change of the secondary-slit-to-sample distance.

Other systematic errors come from coarse grained materials or small samples. Here, only partial regions in the gauge volume contribute to the diffracted signal resulting in a peak shape not representative for the stress condition (Fig. 7 b). Low grain statistics can be improved by measurements of crystallographic planes with high multiplicity and rotation of the sample to increase the number of grains fulfilling the Bragg condition.

Diffraction patterns of multiphase materials usually include several peaks from different microstructural phases. In this case the secondary slit can produce a phase-sensitive systematic problem. The diffraction peaks of two hypothetical phases result in a "splitting" of the gauge volume dependent on the diffraction angle as shown in Fig. 7 c). Relative peak shifts occur if the secondary-slit-to-sample distance is changed, resulting in the measurement of pseudo micro stresses. This problem can be overcome using samples smaller than the gauge volume, with necessarily equally dimensioned reference samples, or by collimation of the diffracted beam.

In TOF neutron diffraction experiments the path length differences in the gauge volume cause comparable absorption and coarse grain influences on the peak positions but these can be neglected due to the long sample-detector path length in comparison with the gauge volume (Santisteban, 2008). The biggest advantage of TOF diffraction is the acquisition of complete diffraction patterns in one scan. However, the asymmetric peak shape (moderator effect) and long counting periods are the limiting factors for this method.

5. Evolution of internal stresses during heat treatment and thermal cycling of MMC

Examples of ex situ and in situ investigations to determine the evolution of internal stresses during heat treatment and thermal cycling of MMC are presented in this chapter.

5.1 Ex situ investigations

5.1.1 Macro-stresses

Annealing processes are known as one of the simplest ways to reduce the level of macrostresses in metallic materials and MMC. When the temperature is high enough to allow thermal relaxation processes, the plastic deformation gradients generated during thermo-mechanical processing, e.g. after quenching, decrease following a exponential decay with time. This is shown in Fig. 8 a) and b) for a cylindrical sample of 6061/SiC/15w with an aspect ratio of about two and a Ti6Al4V/TiB+TiC/8p disc of 15 mm diameter and 3 mm height, respectively. The stress relaxation in 6061/SiC/15w starts with a high tensile stress, while the initial stress condition is compressive in Ti6Al4V/TiB+TiC/8p. The magnitude of stress relaxation depends mainly on the microstructure of the materials and the temperature. However, the progress of the stress decay is independent from the internal architecture of the MMC and from the sign of the stress. For comparison, the stress state reduction after annealing is shown for an unreinforced 6061 Al alloy in Fig. 8 a).

Other authors (Chowdhury et al., 2010) divide this behaviour into two different stages: the first one (initial strong relaxation) is related to a mechanical transient loss and the second one (progressive relaxation) to the microstructural evolution. Although the stress decay is observed for both the MMC and the unreinforced matrix, the presence of the reinforcement

reduces the magnitude of the relaxation of the macrostresses (Fig. 8). On the one hand, the higher dislocation density in the matrix acts as a barrier for dislocation movement. These extra dislocations are mainly the geometrical ones necessary to accommodate the matrix around reinforcement when deformation progresses. This effect is accompanied by the elastic strain fields introduced around the reinforcement. The load transfer from matrix to the stiffer (ceramic or intermetallic) discontinuous reinforcement decreases the amount of stress in the metallic matrix that can act as the driven force for relaxation during annealing.

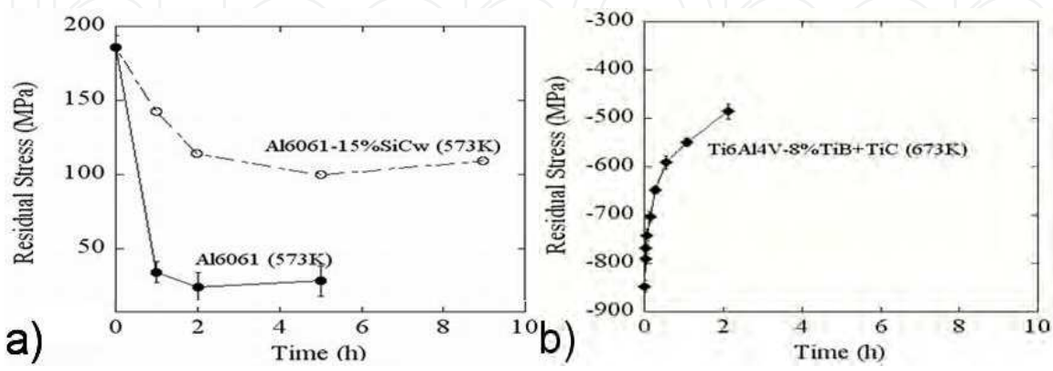

Fig. 8. Axial macrostress decay with annealing time for: a) PM Al alloys 6061 and 6061/SiC/15w at 300 °C (P. Fernández et al., 2005), and b) a disc shape sample of a Ti6Al4V/TiB+TiC/8p (Xie et al., 2005) at 400 °C.

As described above, the macrostress relaxation in lightweight MMC presents a similar stress decay. The relaxation of deviatoric and hydrostatic stress components usually differs in discontinuously reinforced composites. In particular, the hydrostatic component in the matrix of the MMC relaxes slower than in the corresponding unreinforced alloy (Fig. 9). This trend is similar to that found when the creep effects in these materials are compared (Bruno et al., 2004). This fact has not been completely explained yet and more work is needed to understand the correlation between this difference and material's microstructure.

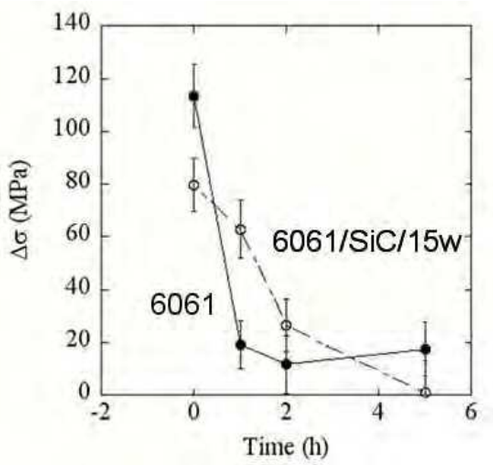

Fig. 9. Evolution of the stress difference between deviatoric and hydrostatic residual stress components during annealing for a 6061/SiC/15w and its corresponding unreinforced 6061 aluminium alloy matrix.

5.1.2 Type II microstresses

Type II microstresses in lightweight MMCs are directly related to their microstructure. The reinforcement architecture (content, size, morphology, distribution, etc.) determines the magnitude of internal stresses in these materials. (Fernández et al., 2011) showed that for PRM with a small interparticle distance (typically 5 μm) the original stress state is conserved almost unaltered after heat treatments. Small interparticle distance can be obtained either by a high reinforcement content (typically > 25vol%) and/or by small particle size (typically >2 μm). The relaxation of internal microstresses is compared in Fig. 10 for materials with different interparticle distances subjected to an overageing heat treatment. For the PRM summarized in Fig. 10, both ingot metallurgy (IM) materials, 2014/Al_2O_3/15p (=W2A15A) and 6061/Al_2O_3/15p (=W6A15A), present an interparticle distance of about 50 μm. The PM 6061/SiC/15w=E219 exhibits a mean interparticle distance of around 5 μm. For the IM MMC (W2A15A and W6A15A), with large interparticle distances, an almost complete relaxation is achieved (Fig. 10 a) and b). However, there is no relaxation in the PM 6061/SiC/15w because dislocation movement is hindered by nanometric Al_2O_3 dispersoids introduced during the PM process (Fig. 10 c).

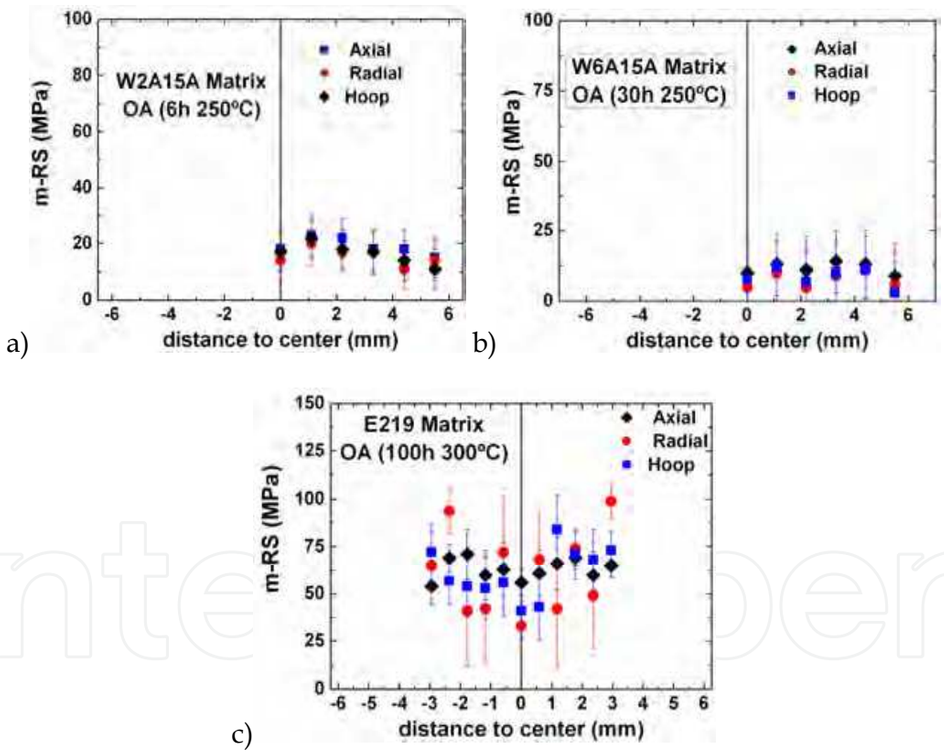

Fig. 10. Relaxation of microstresses after thermal treatment for: a) IM 2014/Al_2O_3/15p, b) IM 6061/Al_2O_3/15p, c) PM 6061/SiC/15w (Fernández et al., 2011).

It is worthy to mention that there are some materials that present an evolution of the internal stresses at room temperature. A typical example is the 7075 Al alloy that undergoes relaxation of internal stresses at room temperature during periods as long as 2 months (Linton et al., 2008). This phenomenon is explained by the ageing of this alloy at room temperature. In other cases, is the application of some specific thermomechanical processes,

such as severe plastic deformation, that allows this room temperature relaxation process. For example, there exists a sigmoidal stresses decay much less pronounced than in the case of the small cylindrical samples shown in Fig. 8 a) (Woo et al., 2009). Since the time-dependent decrease of internal stresses was only observed in the nugget of a friction stir welded part, this evolution must be explained by the microstructural characteristics of this particular zone of the material undergoing natural aging. The presence of high concentrations of vacancies, atoms in solid solution and a large numbers of grain boundaries, may explain this process (Woo et al., 2009).

5.2 In situ determination of microstresses during thermal cycling of lightweight MMC

Insulated gate bipolar transistors (IGBT) are developed for high power applications in hybrid vehicles or railway traction (Baliga, 1979). These sealed IGBT modules consist of semiconducting chips mounted on a ceramic insulator which is soldered onto the baseplate.

The power reaches tens of megawatts concentrated in the small Si chips from which the heat produced must be dissipated through the baseplate into a heat sink. Therefore, base plate materials with high thermal conductivity (TC) and low coefficient of thermal expansion (CTE) are required to avoid delamination and thermal fatigue damage. This can be achieved using MMC formed by an aluminium matrix reinforced with high volume fractions of SiC particles or diamond (CD) particles (> 60 vol.%) to combine the thermal properties of Al (TC_{Al} ~ 250 W/mK, CTE_{Al} ~ 25 ppm/K) with those of SiC (TC_{SiC} ~ 140 W/mK, CTE_{SiC} ~ 5 ppm/K) or CD (TC_{CD} ~ 1000 - 2000 W/mK, CTE_{CD} ~ 1 ppm/K). Such PRM can be produced by liquid metal infiltration (gas pressure infiltration or squeeze casting), where a densely packed particle preform with mono-, bi-, trimodal particle size distributions (Ø ~ 5 – 200 µm) is infiltrated with the melt (Al, AlSi7, AlSi7Mg) (Huber et al., 2006). An AlSi7Mg/SiC/70p composite with a trimodal particle size distribution and voids in between the large SiC particles is shown in Fig. 11 a). In this MMC, with an AlSi7 matrix, the SiC particles are interconnected by eutectic Si bridges (Schöbel et al., 2010). These bridges result in the formation of an ICM with a 3D Si-SiC network embedded in the α-Al matrix.

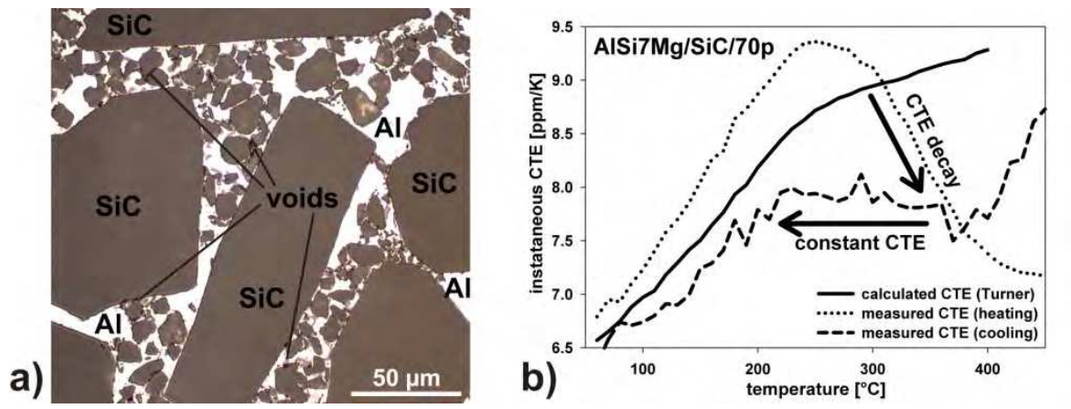

Fig. 11. a) Light optical micrograph of AlSi7Mg/SiC/70p with voids (dark) in the Al matrix (bright) between the SiC particles and b) measured instantaneous CTE(T) compared with that calculated by the thermo-elastic Turner-model (Huber, 2006).

The instantaneous CTE of AlSi7Mg/SiC/70p was investigated in (Huber et al. 2006), where an anomalous behaviour was observed above 200 °C which did not fit to the predictions of

classical thermo-elastic models (Turner, 1946) (Fig. 11 b). A combination of in situ angle dispersive neutron diffraction and in situ synchrotron tomography experiments were performed (Schöbel et al., 2011) to explain this behaviour in terms of internal stresses generated during thermal cycling of the ICM. As explained previously, internal stresses can relax at elevated temperatures. Therefore, short acquisition times in the range of minutes are required for an overall heating / cooling rate comparable to the service conditions of the MMC. Another restrictive property for diffraction studies of these materials is presented by the coarse grains of the α-Al that requires the use of large gauge volumes (> 100 mm²) to increase the grain statistics (see section 3.4.2).

The microstresses obtained by in situ neutron diffraction in an AlSi7/SiC/60p PRM during two thermal cycles (RT – 350°C) are shown in Fig. 12. High hydrostatic compressive stresses up to – 120±80 MPa are generated in the α-Al matrix during heating to 350°C. These stresses invert at ~ 100°C during cooling and become tensile down to room temperature (~ 50°C). The initial tensile stress level at RT ~ 100 MPa increases after the first cycle to ~ 170±70 MPa.

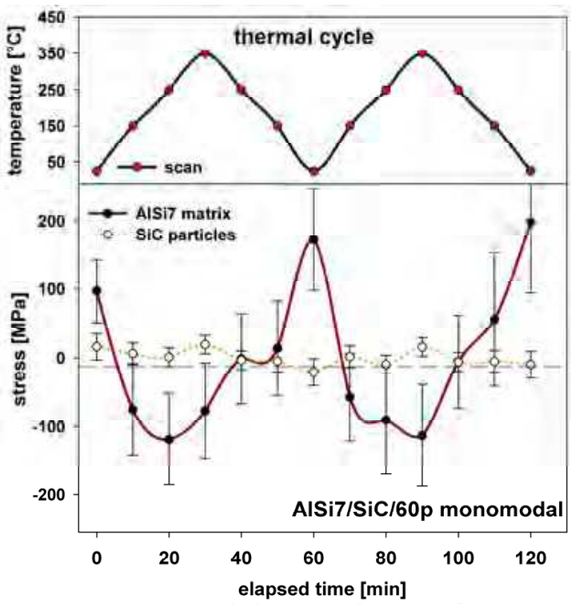

Fig. 12. In situ neutron stress measurement during thermal cycling of AlSi7/SiC/60p (RT – 350°C) showing the stress changes in the α-Al and in the particle stresses (Schöbel et al. 2011).

Synchrotron tomography with (1.4µm)³/voxel of an AlSi7Mg/SiC/70p composite gives information on the evolution of the void volume fraction during thermal cycling (RT – 400°C). Fig. 13 a) shows voids in the AlSi7Mg matrix between large SiC particles. Voids are formed in MMC with a large CTE mismatch between the components and high reinforcement volume fractions during cooling after infiltration even if perfectly infiltrated (Schöbel et al., 2011). Fig. 13 b) shows that the voids close during heating and reopen after cooling. Only voids > (~ 5µm)³ are resolved by the produced tomographies, therefore the given volume fractions only indicate the relative change reliably. During thermal cycling large microstresses between the particles and the matrix (CTE mismatch) change the void volume fraction by visco-plastic matrix deformation (Nam et al., 2008) as indicated by the 2D finite element analysis presented in Fig. 14. The matrix embedded in a 3D reinforcement

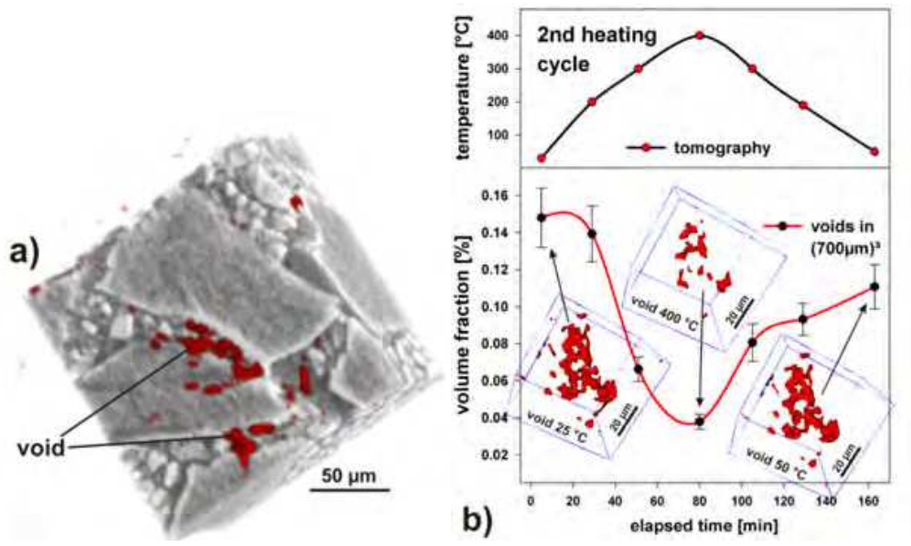

Fig. 13. Voids in an AlSi7Mg/SiC/70p composite during thermal cycling (RT – 400 °C). a) A single void between large SiC particles compared to b) evolution of the void volume fraction during thermal cycling (Schöbel et al. 2011).

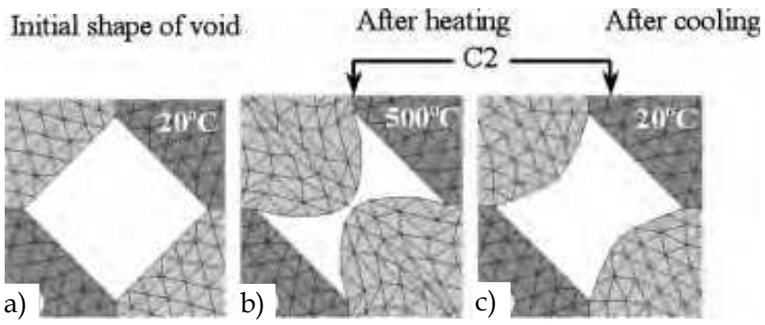

Fig. 14. The change of volume fraction and shape of a void (white) in an ICM formed by SiC (dark grey) and Al (light grey) obtained by finite element analysis: a) 0.25 vol.% void at initial zero stress shrinks to b) 0.103 vol.% after first heating and c) increases to 0.199 vol.% after the following cooling (Nam et al., 2008).

structure expands during heating and closes the voids (CTE decay in Fig. 11 b) which reopen during cooling (constant CTE region in Fig. 11 b) accommodating the volume mismatch.

In the case of a pure Al matrix without Si content, lower stress amplitudes and inverse void kinetics are observed. This was shown using the same experimental procedure, namely in situ neutron diffraction with synchrotron tomography during thermal cycling, for Al/CD/60p and AlSi7/CD/60p composites. The results are shown in Fig. 14. AlSi7/CD/60p behaves similar to AlSi7/SiC/60p with hydrostatic compression up to ~ -120±20 MPa closing the voids during heating, going into to ~ 120±20 MPa tensile stress at RT in which the voids reopen again. In Al/CD/60p, without eutectic Si connecting the diamond particles, low micro stress amplitudes were observed (Schöbel et al., 2010) together with an increase in void volume fraction during heating and decrease during cooling owing to the capability of the matrix to expand in a composite with isolated particles only touching each other.

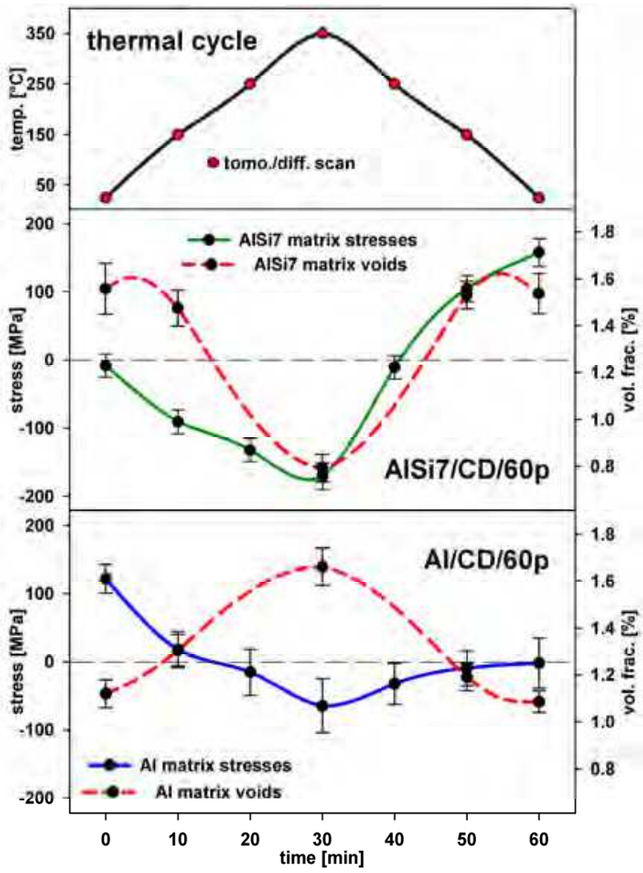

Fig. 15. Evolution of the microstresses in α-Al and of the matrix voids during thermal cycling of Al/CD/60p and AlSi7/CD/60p composites (Schöbel et al. 2010).

6. Evolution of internal stresses during deformation of lightweight MMC

In the present chapter, the evolution of internal stresses during plastic deformation of MMC is presented. Some examples of ex situ and in situ investigations will be summarized in order to describe the main features of this topic.

6.1 Macro-stresses

Similarly to the case of annealing heat treatments, when a material containing residual stresses is deformed, internal stresseses opposite to the applied stress can relax following a exponential decay as deformation progresses. This phenomenon has been extensively studied during the last decade (Levy-Tubiana et al., 2003). It is well establish that during early stages of plastic deformation, typically below 2%, the initial residual stresses are almost totally relaxed. After this initial stage the stress relaxation become less pronounced, like in the case of annealing (see section 4.1). However, after some degree of cumulative deformation, the internal structure of the material is changed by dislocation multiplication, forest dislocations, subgrains, etc. imposing new strain gradients increasing the general residual stress level (R. Fernández et al., 2005). As in the case of thermal relaxation, the behaviour of the deviatoric and hydrostatic components of the macrostresses evolves in a different manner depending on the

microstructure. The results obtained for some discontinuously whisker reinforced MMC with the whiskers oriented preferably along the extrusion direction are shown in Fig. 16. Here, the deviatoric component relaxes completely after a certain value of deformation, while the hydrostatic component increases due to the new plastic strain gradients (P. Fernández et al., 2005). The relaxation behaviour of a conventional unreinforced 2024 IM Al alloy is shown for comparison. It is shown that the presence of reinforcement particles, introduce a higher residual stress level and a higher increase of the hydrostatic component progressing with deformation, mainly due to microstresses induced by geometrical necessary dislocations.

Apart from the effect of microstructural features as reinforcement size, aspect ratio and distribution, imposing slight modifications to the exponential decay of the residual stresses (Fig. 16), the most important difference between the described materials can be related to the processing route. Thus, in the case of the IM materials, the IM 6061/ Al_2O_3/15p MMC and the unreinforced 2024 IM Al alloy, the stress relaxation is more pronounced than in the PM 6061/SiC/15w (C38, C45).

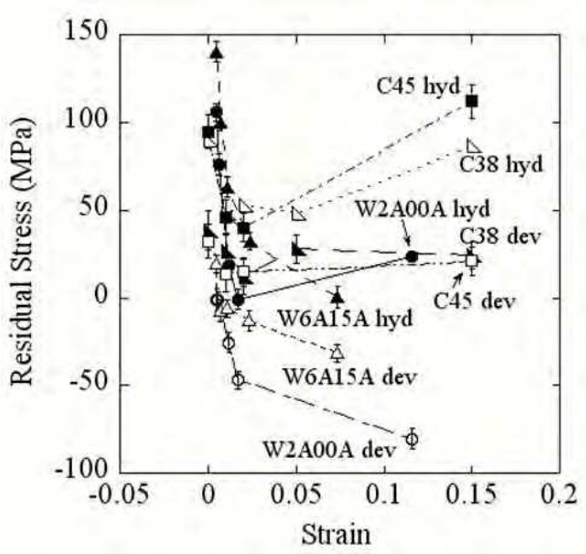

Fig. 16. Residual stress evolution (hyd = hydrostatic, dev = deviatoric) in the matrix of PM 6061/SiC/15w (C38, C45), IM 6061/ Al_2O_3/15p (W6A15A) and 2024 IM alloy (W2A00A) (R. Fernández et al., 2005).

6.2 Microstresses

The evolution of the microstresses with plastic deformation is different from that of the macrostresses. In particular, in PM discontinuously reinforced 6061/SiC/15w with the extrusion direction coinciding with the axial residual stress component, the hydrostatic component of the microstresses continuously relaxes to strain values as high as 15% (Fig. 17). However, the deviatoric microstresses remain constant, within the error bars, as it is shown in Fig. 17.

The fact that microstresses become totally deviatoric after some degree of plastic deformation accounts for the relevance of the activity of geometrically necessary dislocations (GND). In the PM PRM, a part of the reinforcement population is aligned along

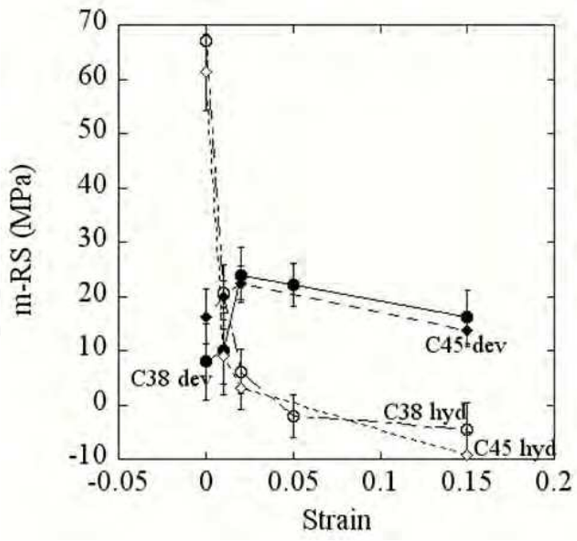

Fig. 17. Hydrostatic (hyd) and deviatoric (dev) microstress evolution in the aluminium phase with plastic deformation for two PM 6061/SiC/15w MMC (C38, C45) (R. Fernández et al., 2005).

the extrusion axis. Therefore, as the GND are mainly at the ends of the whiskers, the microstresses become predominantly deviatoric. This is the case for fibre reinforcements, particularly for short fibres with aligned fibre orientation. The relaxation processes are especially interesting in the case of metal matrix composite with random planar short fibre distribution. Such composites with a relatively low volume fraction of reinforcement (< 30 vol%) are in many cases more attractive, from a mechanical point of view, than composites with a high content of aligned whiskers or continuous fibres because they can be used under multiaxial loading conditions (Hutchinson et al., 1993; Dragone et al., 1991). It has been demonstrated that the mechanical behaviour and the creep properties depend on the direction of the stress with respect to the fibre plane (parallel or transverse to the fibre plane) and the sign of the stress (tension or compression) (Garces et al., 2006b; Garces et al, 2007). During plastic deformation, the MMC stores elastic strain energy within the fibres and when the load is removed the matrix is deformed in the opposite direction. In the case where the fibres were loaded in tension/compression, the matrix surrounding the fibre rapidly unloads elastically and goes into elastic compression/tension. At this stage, the fibre is still in elastic tension/compression. From this point onwards, fibres can only be further unloaded when backflow occurs in the matrix.

The plastic deformation of short-fibre reinforced metals is strongly affected by two competitive mechanisms which occur at the same time: i) the load transfer from the matrix to stiff short fibres under an applied load and ii) the internal damage reducing the load-bearing capacity of the fibres. The internal damage mechanisms reported in the literature are fibre fragmentation, buckling and debonding, as well as void formation at the fibre / matrix interface. The damage mechanisms reduce the capacity to store load by the fibre and, therefore, the internal stresses change depending on the direction and sign of the stress. Fig. 18 shows the evolution of the von Mises internal stress in an $Al/Al_2O_3/15s$ SFRM for three cases: tensile (T) / compressive (C) stress in the direction parallel (P) to the fibre plane (TP and CP, respectively) and compressive stress in a direction perpendicular to the fibre plane

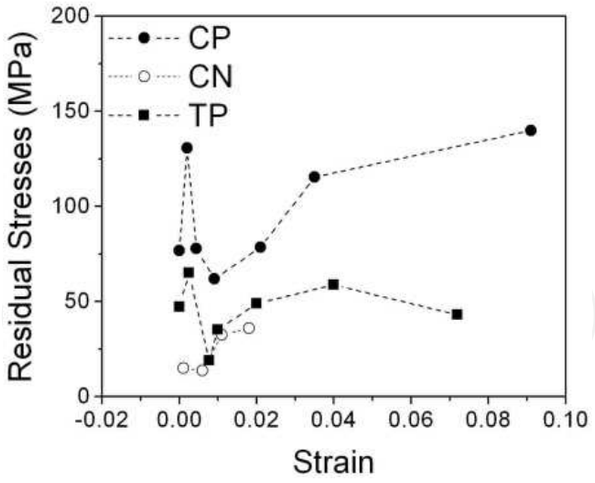

Fig. 18. Von Mises stress in an Al/Al_2O_3/15s SFRM as a function of pre-strain accumulated in the composite for the three loading modes: CP (compression in plane), CN (compression out of plane) and TP (tension in plane) (Garcés et al., 2006b).

(CN). It is important to point out that the von Mises stress in all the cases does not start from zero stress since initial residual stresses generated during the fabrication step pre-exist in the composite. Furthermore, the residual stresses in the CP plane are higher than the CN and TP cases, which are similar. This fact is caused by internal damage, which is less in the case of the compressive direction (CP). On the one hand, in the case of the TP mode, the fibres are mainly loaded in tension, and break earlier or suffer debonding. On the other hand, fibres in the CP and CN modes are slightly buckled, which is not as damaging as tension.

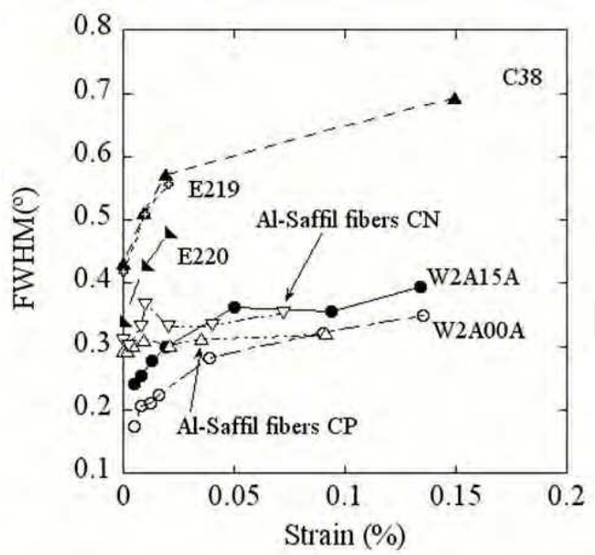

Fig. 19. Evolution of the microstresses represented by FWHM of the neutron diffraction peaks during plastic deformation of some Al matrix composites and their corresponding unreinforced alloys: PM 6061/SiC/15w extruded using a conical (C38) and a flat-shaped extrusion tool (E219); PM unreinforced 6061 alloy (E220); IM 6061/Al_2O_3/15p (W6A15A) and IM 2024 alloy (W2A00A) (R. Fernández et al., 2005).

As the central position of the diffracted peak is related to the lattice parameter, the Full Width at Half Maximum (FWHM) of a diffraction peak quantifies the scatter introduced in the diffraction process by fine grains and type III microstresses, mainly by the dislocation density. The FWHM is shown in Fig. 19 for some MMC as a function of applied strain (Garcés et al., 2006b; R. Fernández et al., 2005). The FWHM increases with the dislocation multiplication process as plastic deformation proceeds. In particular, PM materials present a more pronounced evolution of the FWHM. In the IM 2124/Al_2O_3/15p PRM and Al/Al_2O_3/15s SFRM this increment is weaker. It is interesting to point out that this fact seems to be independent of the fibre aspect ratio and it is more related with the fabrication route. Nanometric Al_2O_3 dispersoids introduced during the PM process anchor dislocations suppressing annihilation processes as plastic deformation advances.

6.3 Load partition in lightweight MMC with three-dimensional interpenetrating structures

Neutrons have been extensively used to follow in situ the evolution of internal stresses in MMC during deformation (see e.g. Withers et al., 1989; Shi et al., 1997; Daymond et al., 1999). Recently, there has been a great interest in ICM due to a more rigid and efficient reinforcement effect that these composites offer, especially at high temperatures (e.g. Roy et al., 2011; Long et al., 2011; Requena et al., 2011). The microstructure of these interconnected systems is usually characterized by a random distribution of ceramic and/or intermetallic phases, but infiltrated preforms of random planar oriented short fibres can present preferred orientations of the reinforcement (Roy et al., 2011; Requena et al., 2009). Within this group of materials, the composites reinforced with short fibres interconnected with eutectic Si and aluminides (see Fig. 1 c) are of technological interest and have been used to locally reinforce diesel pistons. As we commented briefly above, such composites exhibit a more balanced property profile, are less anisotropic and present a better mechanical response under multiaxial loading conditions.

The strength of an AlSi12/Al_2O_3/20s ICM was investigated in (Requena et al., 2009a) by in situ neutron diffraction during compression tests. Besides the high interconnectivity that is usually obtained in the eutectic Si in the as cast (AC) condition (Lasagni et al., 2007) this phase forms bridges between the ceramic short fibres (Requena & Degischer, 2006). Thus, an IMC with an interconnected 3D reinforcement of eutectic Si and Al_2O_3 short fibres is obtained. The strength, stability and degree of interconnectivity of this 3D structure are sensitive to the amount and size of the Si bridges, which can be modified by heat treatment (Lasagni et al, 2008). The composite was therefore investigated in AC condition and after a solution treatment (ST) at 540°C during 4 hours to study the effect of different Si-short-fibres architectures on the strength.

The Si bridges connecting the short fibres can be seen in Fig. 20 a) for AlSi12/Al_2O_3/20s-AC. The large amount of Si bridges results in a 3D structure formed by the Al_2O_3 short fibres and the eutectic Si that remains together after leaching out the Al matrix. After the spheroidisation treatment, the Si forms round particles, most of which stick to the interface of the short fibres (see Fig. 20 b) but the number of Si bridges decreases as well as the connectivity of the 3D structure. The highest strength is exhibited by the AlSi12/Al_2O_3/20s-AC composite (Requena et al., 2009a). The stress directions considered for the stress partition analysis as well as the load direction are shown schematically in Fig. 21 taking into

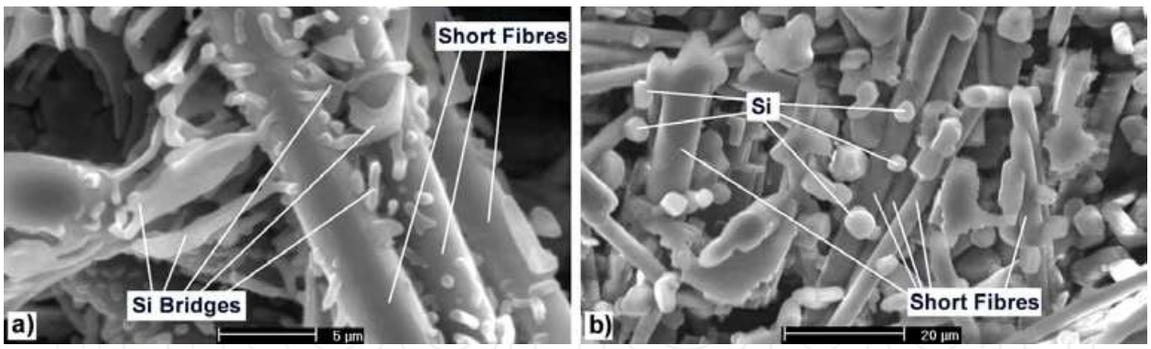

Fig. 20. Morphology of the Si-short-fibres structure in an AlSi12/Al_2O_3/20s after deep etching: a) AC condition, where fine elongated eutectic Si bridges connect the short fibres and b) ST condition (lower magnification), where Si forms round particles, which stick to the interface of the ceramic short fibres (Requena et al., 2009a).

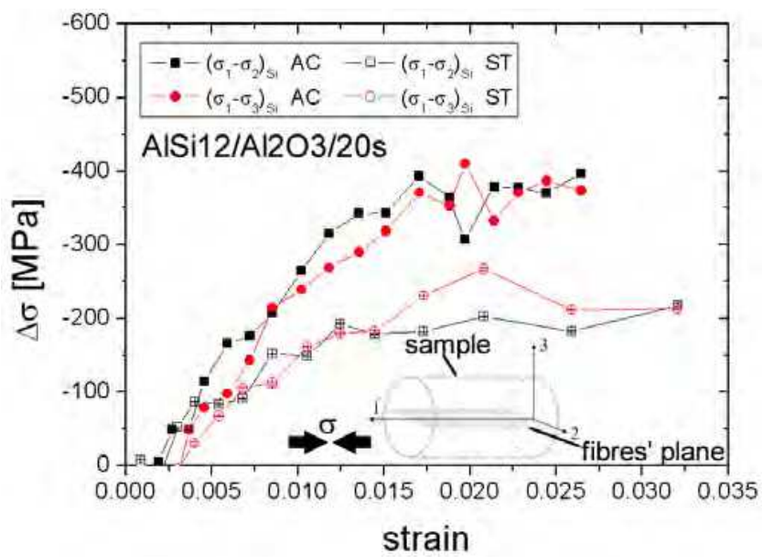

Fig. 21. Evolution of the stress differences (σ_1-σ_3) and (σ_1-σ_2) in AlSi12/Al_2O_3/20s determined by in situ neutron diffraction for the eutectic Si in the AC and 540°C/4h conditions as a function of the applied compressive strain. The geometry of the sample and the orientation of the fibres' plane (1-2) with respect to the applied stress σ (1) are indicated (Requena et al. 2009a).

account the shape of the samples used for the in situ tests and the orientation of the fibres. Furthermore, Fig. 21 shows the evolution of the stress differences (σ_1-σ_3) and (σ_1-σ_2) obtained during the in situ neutron diffraction experimentes as a function of the applied strain for the eutectic Si in the AC and 540°C/4h conditions. It is observed, that the eutectic Si in the AlSi12/Al_2O_3/20s-AC ICM presents a higher load bearing capacity than the eutectic Si after 540°C/4h. However, the eutectic Si in the ICM carries a smaller portion of load than in the case of the unreinforced AlSi12 alloy (Requena et al, 2009b) although the composite exhibits a higher strength. This is due to the fact that the load is carried by the network formed by short fibres and the eutectic Si in the case of the ICM. A mean field model proposed rationalized the evolution of the principal stress differences and the von-

Mises stress in the aluminium matrix, the eutectic Si and the short fibres (Requena et al., 2009a). The reinforcing effect of the fibres and of the eutectic Si were reflected as well as the reinforcing potential of isolated elongated Si particles. However, this model does not take into account the interconnectivity between the short fibres and the eutectic Si underestimating the load transfer from the matrix to the reinforcement architecture. These results support the need to take into account the interconnectivity of the reinforcing structure to understand the high strength exhibited by these composites, especially at high temperatures.

7. Acknowledgments

M. Hofmann (FRM II), J. Repper (PSI), S. Van Petegem (PSI), A. Evans (ILL), T. Pirling (ILL), R. Wimpory (HZB), C. R. Hubbard (Oak Ridge Nat. Lab.), T. H. Gnäupel-Herold (Nat. Inst. of Stand. and Techn.), S. Y. Zhang (ISIS), A. Paradowska (ISIS), V. Klosek (LLB).

G. Requena and M. Schöbel would like to acknowledge the "K-Project for Non-Destructive Testing and Tomography" supported by the COMET-Program of the Austrian Research Promotion Agency (FFG) and the Province of Upper Austria (LOÖ), Grant No. 820492.

8. Conclusions

The contribution of the neutron diffraction technique to the understanding of the generation and evolution of thermo-mechanically induced residual and internal stresses in lightweight metal matrix composites has been reviewed in the frame of relevant literature. Besides the conclusions corresponding to the specific works described, the following conclusions are withdrawn:

- The neutron diffraction technique has evolved during the last decades to become a well-established technique to measure residual / internal stresses both by ex situ and in situ experiments in crystalline multiphase materials. The considerable amount of dedicated state of the art instruments available around the world to external users shows the importance of the neutron diffraction technique for materials scientists.
- Neutron diffraction still presents some advantages to determine internal/residual stresses which are decisive under certain experimental conditions in comparison with the modern high brilliance synchrotron radiation sources, e.g. a larger penetration depth and the possibility to use larger gauge volumes. Furthermore, the modern neutron sources allow now acquisition times of only a few minutes to acquire reliable data, which is crucial for in situ experiments.

9. References

Ashby, M. *Materials Selection in Mechanical Design* (3rd edition), Butterworth-Heinemann, ISBN 075061682, Oxford.

Baliga B.J. (1979). Enhancement and Depletion Mode Vertical Channel MOS Gated Thyristors. *Electronic Letters*, Vol. 15, pp. 645-647.

Behrens, M. (2011). Powder X-ray and neutron diffraction, Lecture series: Modern Methods in Heterogeneous Catalyst Research.

Birchall, J.; Stanley, D. Mockford, M.; Pigott, G. & Pinto, P. (1988). The Toxicity of Silicon Carbide Whiskers, *J Mater Sci Letters*, Vol. 7, 350-352.

Brendel, A.; Popescu, C.; Köck, T. & Bolt, H. (2007). Promising composite heat sink material for divertor of future fusion reactors, *J Nuclear Mater,* Vol. 367-370 B, pp. 1476-1480.

Bruno, G.; Fernández, R. & González-Doncel, G. (2004). Relaxation of the residual stress in 6061Al-15 vol.% SiCw composites by isothermal annealing *Mat Sci Eng A,* Vol. 382, No. 1-2, pp. 188-197.

Brückel, T.; Heger, G.; Richter, D. & Zorn, R. (2005). *Neutron Scattering, Matter and Materials* 28, Jülich.

Buffa, G.; Fratini, L.; Pasta, S.; Shivpuri, R. (2008). *CIRP annals*, Vol. 1, No. 57, 287.

Carpenter, JM. (2008) *Neutron Sources for Materials Research.* Tenth international School on Neutron and X-ray Scattering, University of Chicago.

Chowdhury,A.; Mari,D. & Schaller,R. (2010).Thermal stress relaxation in magnesium matrix composites controlled by dislocation breakaway. *Comp Sci Tech,* Vol.70, pp. 136-142.

Daymond, M.R.; Lund, C.; Bourke, M.A.M. & Dunand, D.C. (1999). Elastic phase-strain distribution in a particulate-reinforced metal-matrix composite deforming by slip or creep *Metall Mater Trans A*, Vol. 30, pp. 2989-2997.

Degischer, H. P. (1997). Innovative light metals: metal matrix composites and foamed aluminium, *Materials & Design*, Vol. 18, pp. 221-226.

Dragone, T.L.; Schlauchtmann, J.J. & Nix, W.D. (1991). Processing and creep characterization of a model metal matrix composite: Lead reinforced with nickel fibers. *Metall Trans. A* 22, No. 5, pp. 1029-1036.

Dutta, I.; Allen, S. & Hafley, J. (1991). Effect of reinforcement on the aging response of cast 6061 Al-Al_2O_3 particulate composites *Metall Trans A*, Vol. 22, No. 11, pp. 2553-2563.

CES Edupack Aerospace Edition, October 2011, Available from: http://www.grantadesign.com/education/content.htm.

Fernández, P. ; Fernández, R. ; González-Doncel, G. & Bruno, G. (2005). Correlation between matrix residual stress and composite yield strength in PM 6061Al–15 vol% SiCw. *Scripta Mater,* Vol. 52, No. 8, pp. 793-797.

Fernández, R.; Bruno, G. & González-Doncel, G. (2005). Residual stress evolution with compressive plastic deformation in 6061Al–15 vol.% SiCw composites studied by neutron diffraction *Mat Sci Eng A,* Vol. 403, No. 1-2, pp. 260-268.

Fernández, P.; Bruno, G.; Fernández & R. González-Doncel G. (2011). Fifth AUSE user meeting. Valencia 7-9 September 2011.

Fitzpatrick, M.E. & Lodini, A. (2003) *Analysis of Residual Stress by Diffraction using Neutron and Synchrotron Radiation*, Taylor & Francis, London.

MMC-ASSESS, October 2011, Available from: http://mmc-assess.tuwien.ac.at.

FRM II. STRESS-SPEC Eigenspannungs- und Texturdiffraktometer, October 2011, Available from: http://www.frm2.tum.de/wissenschaftliche-nutzung/diffraktion/stress-spec/

Garcés, G.; Bruno, G. & Wanner, A. (2006). Residual stresses in deformed random-planar aluminium/Saffil short-fibre composites *Mat Sci Eng A*, Vol. 417, No. 1-2, pp. 73-81.

Garcés, G.; Bruno, G. & Wanner, A. (2006) Residual stresses in deformed random-planar aluminium/Saffil® short-fibre composites deformed in different modes *Int J Mat Res,* Vol. 97, No. 10, pp. 1312-1319.

Garcés, G. Bruno & G. Wanner, A. (2007) Load transfer in short fibre reinforced metal matrix composites *Acta Mater,* Vol. 55, No. 16, pp. 5389-5400.

Hofmann, M.; Seidl, G.A.; Rebelo-Kornmeier, J.; Garbe, U.; Schneider, R.; Wimpory, R.C.; Wasmuth, U. & Noster, U. (2006). The new materials science diffractometer STRESS-SPEC at FRM-II. *Mat Sci Forum,* Vol. 524-525, pp. 211-216.

Huber, T.; Degischer, H.P.; Lefranc, G. & Schmitt, T. (2006). Thermal expansion studies on aluminium-matrix composites with different reinforcement architecture of SiC particles *Comp Sci Tech,* Vol. 66, No. 13, pp. 2206-2217.

Hutchinson, J. & McMeeking, R. (1993). *Continuous models for deformation: discontinuous reinforcement*. Suresh, S. Mortensen, A. Needleman, A. editors. Fundamentals of metal matrix composites. Butterworth-Heinemann.

Hutching, M.T.; Withers, P.J.; Holden, T.M. & Lorentzen T. (2005). *Introduction of the characterization of residual stress by neutron diffraction*. Taylor and Francis Group.

HZB. Neutron Residual Stress/Materials diffractometer, October 2011, Available from: http://www.helmholtz-berlin.de/forschung/funkma/werkstoffe/methoden/neutronendiffraktion_en.html

ILL. Strain imager for engineering applications SALSA, October 2011, Available from: http://www.ill.eu/instruments-support/instruments-groups/instruments/salsa/

ISIS. Engin-X Engineering materials beamline, October 2011, Available from: http://www.isis.stfc.ac.uk/instruments/engin-x/

KENS. SIRIUS (High resolution and high intensity powder diffractometer), October 2011, Available from: http://neutron-www.kek.jp/kens2/kens_e/spectrometer/sirius.html

Lasagni, F.; Lasagni, A.; Marks, E.; Holzapfel, C.; Mücklich, F. & Degischer, H.P. (2007). Three-dimensional characterization of 'as-cast' and solution-treated AlSi12(Sr) alloys by high-resolution FIB tomography. *Acta Mater*, Vol. 55, pp. 3875-3882.

Lasagni, F.; Acuña, J. & Degischer, H.P. (2008). Interpenetrating Hybrid Reinforcement in Al_2O_3 Short Fiber Preforms Infiltrated by Al-Si Alloys, *Met Mat Trans A,* Vol. *39*, No. 6, pp. 1466-74.

Levy-Tubiana, R.; Baczmanski, A. & Lodini, A. (2003). Relaxation of thermal mismatch stress due to plastic deformation in an Al/SiCp metal matrix composite. *Mat Sci Eng A*, Vol. 341, No. 1-2, pp. 74-86.

Leyens, C.; Kocian, F.; Hausmann & J. Kaysser, W.A. (2003). Materials and design concepts for high performance compressor components, *Aero Sci Tech,* Vol. 7, pp. 201-210.

Linton, V. & Ripley, M.I. (2008). Influence of time on residual stresses in friction stir welds in agehardenable 7xxx aluminium alloys *Acta Mater,* Vol. 56, No. 16, pp. 4319-4327.

LLB. Two-Axis Strain Diffractometer "DIANE", October 2011, Available from: http://www-llb.cea.fr/en/fr-en/pdf/g52-llb.pdf

Long, J.; Li, W.; Chen, S.; Lin, J. & Zeng, Y. (2011). Interface Study of Short Mullite Fiber Reinforced Al-Cu-Si Alloy Composites. *Adv Mater Res,* Vol. 150-151, pp. 1574-1579.

Los Alamos National Laboratory. Spectrometer for Materials Research at Temperature and Stress, October 2011, Available from: http://lansce.lanl.gov/lujan/instruments/SMARTS/

Nam, T.H.; Requena, G. & Degischer, P. (2008). Thermal expansion behaviour of aluminum matrix composites with densely packed SiC particles. *Compos Part A*, Vol. 39, No. 5, pp. 856-865.

NIST. The BT8 Residual Stress Diffractometer, October 2011, Available from: http://www.ncnr.nist.gov/instruments/darts/

Oak Ridge National Laboratory. Neutron Residual Stress Mapping Facility (HB-2B), October 2011, Available from: http://neutrons.ornl.gov/instruments/HFIR/HB2B/

Noyan, I.C. & Cohen, J.B. (1987). *Residual stress. Measurement by diffraction and Interpretation* Springer-Verlag New York Inc.

Peters, P.; Hemptenmacher, J. & Schurmann, H. (2010). The fibre/matrix interface and its influence on mechanical and physical properties of Cu-MMC. *Comp Sci Tech,* Vol. 70, No. 9, pp. 1321-1329.

Pirling. T.; Bruno, G. & Withers, P.J. (2006). SALSA, a new concept for strain mapping at the ILL. *Mat Sci Eng A*, Vol. 437, pp. 139-144.

PSI. POLDI: Pulse Overlap time-of-flight Diffractometer, October 2011, Available from: http://poldi.web.psi.ch/

Pynn R. (2011). Neutron Scattering, Lectures, Los Alamos National Laboratory.

Requena, G. & Degischer, H.P. (2006). Creep behaviour of unreinforced and short fibre reinforced AlSi12CuMgNi alloy. *Mat Sci Eng A*, Vol. 420, No. 1-2, pp. 265-275.

Requena, G.; Garcés, G.; Danko, S.; Pirling, T. % Boller, E. (2009). The effect of eutectic Si on the strength of short-fibre-reinforced Al. *Acta Mater*, Vol.57, No. 11, pp. 3199-3210.

Requena, G.; Garcés, G.; Rodríguez, M.; Pirling, T. & Cloetens, P. (2009). 3D architecture and load partition in eutectic Al-Si alloys. *Adv Eng Mater,* Vol. 11, No. 12, pp.1007-1014.

Requena, G.; Garcés, G; Asghar, Z.; Marks, E.; Staron, P. & Cloetens, P. (2011). The effect of the connectivity of rigid phases on strength of Al-Si alloys. *Adv Eng Mater.*, Vol. 13, No. 8, pp. 674-684.

Roy, S.; Gibmeier, J.; Kostov, V.; Weidenmann, K.A.; Nagel, & A. Wanner, A. (2011) Internal load transfer in a metal matrix composite with a three-dimensional interpenetrating structure *Acta Mater.,* Vol. 59, No. 4, pp. 1424-1435.

Santisteban J.R. et al. Neutrons and Synchrotron Radiation in Engineering Materials Science, WILEY-VCH, Weinheim, 2008.

Schöbel, M.; Degischer, H.P.; Vaucher, S.; Hofmann, M. & Cloetens, P. (2010). Reinforcement architectures and thermal fatigue in diamond particle-reinforced aluminum. *Acta Mater,* Vol. 58, No. 19, pp. 6421-6430.

Schöbel, M.; Altendorfer, W.; Degischer, P.; Vaucher, S.; Buslaps, T.; Di Michiel, M. & Hofmann, M. (2011). Internal stresses and voids in SiC particle reinforced aluminum composites for heat sink applications. *Comp Sci Tech,* Vol. 71, No. 5, pp. 724-733.

Shi, N.; Bourke, M.A.M.; Roberts, J.A. & Allison, J.E. (1997). Phase-stress partition during uniaxial tensile loading of a TiC-particulate-reinforced Al composite *Metall Mater Tran. A,* Vol. 28A, No. 12, pp. 2741-2743.

Stuhr, U. (2005). Time-of-flight diffraction with multiple pulse overlap. Part I: The concept. *Nucl Instrum Meth A,* Vol. 545, pp. 319-329.

Stuhr, U.; Spitzer, H.;Egger, J.; Hofer, A.; Rasmussen, P.; Graf, D.; Bollhalder, A.; Schild, M. Bauer, G. & Wagner W. (2005). Time-of-flight diffraction with multiple frame overlap Part II: The strain scanner POLDI at PSI. *Nucl Instrum Meth A,* Vol. 545, pp. 330-338.

Tjong S. C. & Ma Z.Y. (2000), Microstructural and Mechanical Characteristics of In Situ Metal Matrix Composites *Mat Sci Eng A,* Vol. 29, pp. 49-113.

Wimpory, R.C.; Mikula, P.; Šaroun, J.; Poeste, T.; Li, J.; Hofmann, M. & Schneider, R. (2008). Efficiency boost of the materials science diffractometer E3 at BENSC: one order of

magnitude due to a horizontally and vertically focusing monochromator. *Neutron News*, Vol.19, No. 1, pp. 16-19.

Withers, P.J.; Stobbs, W.M. & Pedersen, O.B. (1989). The application of the Eshelby method of internal stress determination to short fibre metal matrix composites *Acta Metal,* Vol. 37, No. 11, pp. 3061-3084.

Wither, P.J.; Badeshia, H. (2001). Residual stress. Part 1 – Measurement techniques. Mat Sci Tech, Vol. 17, pp. 355-365.

Woo, W.; Feng, Z.; Wang, X.-L. & Hubbard, C.R. (2009). Neutron diffraction measurements of time-dependent residual stresses generated by severe thermomechanical deformation. *Scripta Mater*, Vol. 61, No. 6, pp. 624-627.

Xie, L.; Jiang, C. & Ji, V. (2005). Thermal relaxation of residual stresses in shot peened surface layer of (TiB + TiC)/Ti–6Al–4V composite at elevated temperatures. *Mat Sci Eng A,* Vol. 528, pp. 6478-6483

Young, M.L.; DeFouw, J.; Almer, J.D. & Dunand D.C. (2007). Load partitioning during compressive loading of a Mg/MgB_2 composite. *Acta Mater,* Vol. 55, No. 10, pp. 3467-3478.

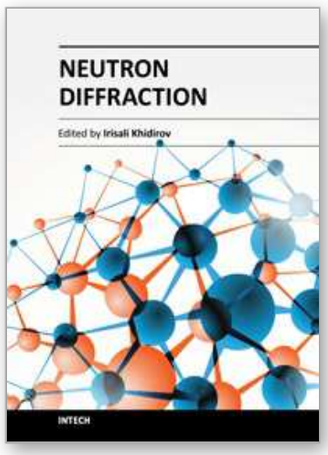

Neutron Diffraction

Edited by Prof. Irisali Khidirov

ISBN 978-953-51-0307-3
Hard cover, 286 pages
Publisher InTech
Published online 14, March, 2012
Published in print edition March, 2012

Now neutron diffraction is widely applied for the research of crystal, magnetic structure and internal stress of crystalline materials of various classes, including nanocrystalls. In the present book, we make practically short excursion to modern state of neutron diffraction researches of crystal materials of various classes. The book contains a helpful information on a modern state of neutron diffraction researches of crystals for the broad specialists interested in studying crystals and purposeful regulation of their service characteristics, since the crystal structure, basically, defines their physical and mechanical properties. Some chapters of the book have methodical character that can be useful to scientists, interested in possibilities of neutron diffraction. We hope, that results of last years presented in the book, can be a push to new ideas in studying of crystalline, magnetic structure and a macrostructure of usual crystal materials and nanocrystals. In turn, it can promote working out of new materials with new improved service characteristics and to origin of innovative ideas.

How to reference

In order to correctly reference this scholarly work, feel free to copy and paste the following:

Guillermo Requena, Gerardo Garcés, Ricardo Fernández and Michael Schöbel (2012). Determination of Internal Stresses in Lightweight Metal Matrix Composites, Neutron Diffraction, Prof. Irisali Khidirov (Ed.), ISBN: 978-953-51-0307-3, InTech, Available from: http://www.intechopen.com/books/neutron-diffraction/determination-of-internal-stresses-in-lightweight-metal-matrix-composites

INTECH
open science | open minds

InTech Europe
University Campus STeP Ri
Slavka Krautzeka 83/A
51000 Rijeka, Croatia
Phone: +385 (51) 770 447
Fax: +385 (51) 686 166
www.intechopen.com

InTech China
Unit 405, Office Block, Hotel Equatorial Shanghai
No.65, Yan An Road (West), Shanghai, 200040, China
中国上海市延安西路65号上海国际贵都大饭店办公楼405单元
Phone: +86-21-62489820
Fax: +86-21-62489821

IntechOpen